

Photothermal Detection of Incipient Dental Caries: Experiment and Modeling

Anna Matvienko^{a,b}, Raymond J. Jeon^{a,b}, Andreas Mandelis*^{a,b}, Stephen H. Abrams^b, Bennett T. Amaechi^c

^aCenter for Advanced Diffusion Wave Technologies, Department of Mechanical and Industrial Engineering, University of Toronto, 5 King's College Road, Toronto, Ontario, M5S 3G8, Canada;

^bQuantum Dental Technologies, 748 Briar Hill Avenue, Toronto, Ontario, M6B 1L3, Canada;

^cDepartment of Community Dentistry, University of Texas Health Science Center at San Antonio, 7703 Floyd Curl Drive, San Antonio, Texas 78229-3900, USA

ABSTRACT

Laser induced photothermal radiometry (PTR) was applied as a safe, non-destructive, and highly sensitive tool for the detection of early tooth surface demineralization. In the experiments, teeth were treated sequentially with an artificial demineralization gel to simulate controlled mineral loss on the enamel surface. Modulated laser light generated infrared blackbody radiation from teeth upon absorption and nonradiative energy conversion. The infrared flux emitted by the treated region of the tooth surface and sub-surface was monitored with an infrared detector twice: before and after treatment. The experiments showed very high sensitivity of the measured signal to incipient changes in the enamel structure, emphasizing the clinical capabilities of the method. In order to analyze the biothermophotonic phenomena in a sample during the photothermal excitation, a theoretical model featuring coupled diffuse-photon-density-wave and thermal-wave fields was developed. The theoretical fits based on the three-layer approach (demineralized enamel + healthy enamel + dentin) allowed fitting thermal and optical properties of the demineralized layer. The theoretical analysis showed that the dentin layer should be taken into account in the fittings.

Keywords: Photothermal radiometry, non-invasive, demineralization, enamel, dentin

1. INTRODUCTION

During the past decades, photothermal techniques have become increasingly popular in the field of non-destructive evaluation of thermal and optical properties of materials. This family of techniques can be used not only for optical and thermal evaluation, but they also have a huge potential for biomedical imaging and detection due to their non-invasive character. Among them, coupled-field (photoacoustic and photothermal) techniques recently attracted much attention since the secondary (acoustic or thermal) signal detection can significantly increase resolution of pure optical diagnostics and imaging, and allows comprehensive and simultaneous analysis of optical and thermal properties of tissue during laser irradiation. This type of analysis is inevitably necessary for a majority of laser-tissue interaction processes.

Both pulsed and frequency-domain modes of photothermal radiometry are based on the thermal infrared response of a medium to a single-pulse (or frequency-modulated) laser irradiation following optical-to-thermal energy conversion. The generated signals carry subsurface information in the form of a temperature depth integral, allowing analysis of the medium well below the range of optical imaging. Based on the measured infrared signal, both optical and

*mandelis@mie.utoronto.ca

thermal characteristics of tissues can be evaluated non-invasively. Pulsed photothermal radiometry was applied to various tissue measurements, including dental enamel.^{1,2} However, the temporal decay of the thermal pulse represents only one signal channel available to analysis, requiring an additional independent optical measurement to extract a reliable set of optical parameters.³

Frequency-domain photothermal radiometry provides two signal channels (amplitude and phase). In this method, harmonically modulated laser beam generates diffuse-photon-density waves in a turbid medium. Following photon migration and scattering, the absorbed fraction of the diffusive light creates an oscillatory temperature (thermal-wave) field, which is detected radiometrically.

The complete theoretical formalism of photothermal radiometry includes the description of two fields: optical and thermal. A method for non-invasive simultaneous optical and thermal characterization of turbid media has been introduced,^{4,5} in which the authors developed a rigorous three-dimensional model for frequency-domain photothermal radiometry, where the diffuse-photon-density field in the laser-irradiated tissue acts as a modulated source for the thermal-wave field. This method was later applied for the optical and thermal evaluation of homogeneous dental enamel.⁶

However, in many cases biological tissues such as skin, teeth, etc. are not homogeneous and should be represented as a layered structure. There are a number of studies on the optical evaluation of a layered medium. Steady-state, time-resolved, and frequency-domain optical fields in a two-layer turbid medium have been examined within the diffusion approximation of the radiative transport equation.⁷⁻¹⁰ These studies demonstrated good potential for estimating the optical properties and/or the layered structure of tissue using the diffusion approximation theory fitted to measured^{7,8} or Monte Carlo simulated^{9,11,12} reflectance data. A Fourier transform-based solution for the diffusion approximation was presented for a two-layered^{9,13} tissue analysis. The authors calculated depth profiles and time-domain dependence of reflectance for a layered matched medium and compared the results to the Monte Carlo generated reflectance profiles.

In this paper, we apply the theoretical formalism developed for the frequency-domain photothermal radiometry of a single-layer turbid medium^{4,5} to the three-layer case and show the capabilities of the model to describe diffuse-photon-density and thermal-wave profiles as a function of the properties of the layers. The comparison of the theoretical profiles to the experimental results on the artificial demineralization of dental enamel leads to evaluation of optical and thermal properties of demineralized teeth as one-dimensional three-layer structures.

The motivation for these studies is the assessment of the capabilities of photothermal radiometry to monitor quantitatively the demineralization of dental enamel due to natural processes, such as by acids produced through bacterial metabolic activities or contained in food and drinks. In fact, early carious lesions, where the demineralization of the underlying enamel crystal structure has just started, are not detectable by conventional visual diagnostics or dental radiographs. In order to improve detection accuracy and to use non-radiographic methods, the application of a laser-induced non-invasive technique, such as the frequency-domain photothermal radiometry, for early detection of caries becomes very promising.

2. EXPERIMENTAL SETUP AND PROCEDURE

In the experiments, teeth (Fig. 1) were treated sequentially with an artificial demineralization gel (0.1M lactic acid, 0.1M NaOH to raise the pH to 4.5, and 6% w/v hydroxyethylcellulose) to simulate controlled mineral loss on the enamel surface. The experimental setup (Fig. 2) included a semiconductor laser (659 nm, 80mW) as a source of the PTR signal. During the experiments, frequency scans were performed at the treatment location.

Here, the diameter of the laser beam was a key issue in order to achieve one-dimensionality of the thermal-wave field, so the adoption of the one-dimensional theory for the analysis of the process would be justified. Preliminary tests showed that 3 mm was the minimal beam width assuring one-dimensional thermal-wave profile.

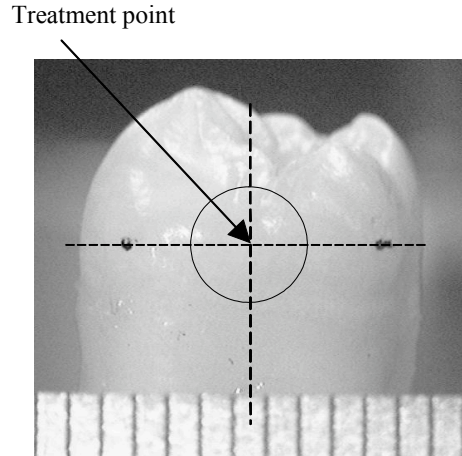


Fig. 1. Tooth sample and treatment spot.

Modulated laser light generated infrared blackbody radiation from teeth upon absorption and nonradiative energy conversion. The infrared flux emitted by the treated region of the tooth surface was focused by two off-axis paraboloidal mirrors and was monitored with a mercury-cadmium-telluride (MCT) infrared detector. The measurements were performed in the frequency-scan mode, i.e. monitoring the output signal as a function of modulation frequency of the incident laser beam. The samples were mounted on LEGO bricks, which ensured their accurate placement in the holders for scanning, and controlled by precision micro-stages. The output signal was acquired automatically using developed instrument control software, so no operator input influenced the results.

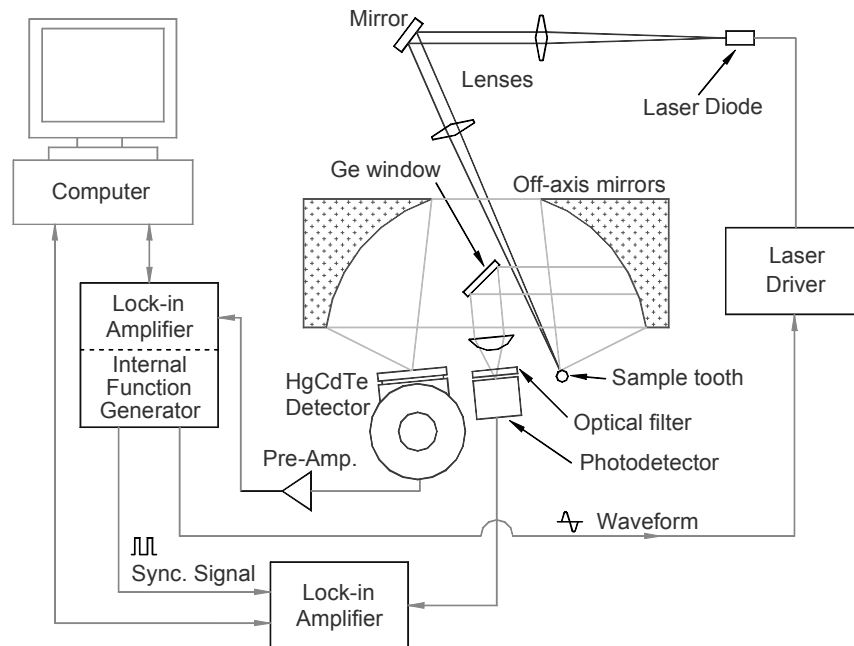


Fig. 2. Experimental setup.

The output voltage was measured at the same spot three times: before and after 2 and 4 days of the demineralization treatment. Due to the change in the properties of enamel in the etched region, the emitted flux profiles changed after each treatment.

3. THEORY

As a result of the incident laser radiation, diffuse-photon-density distribution occurs inside the turbid medium. It can be divided into two components,⁶ namely coherent and diffuse:

$$\Psi_{t_i}(z; \omega) = \Psi_{c_i}(z; \omega) + \Psi_{d_i}(z; \omega) \quad (1)$$

Here and further in the text, the subscript i denotes 1 – demineralized layer, 2 – intact enamel, 3 – dentin (Fig.3).

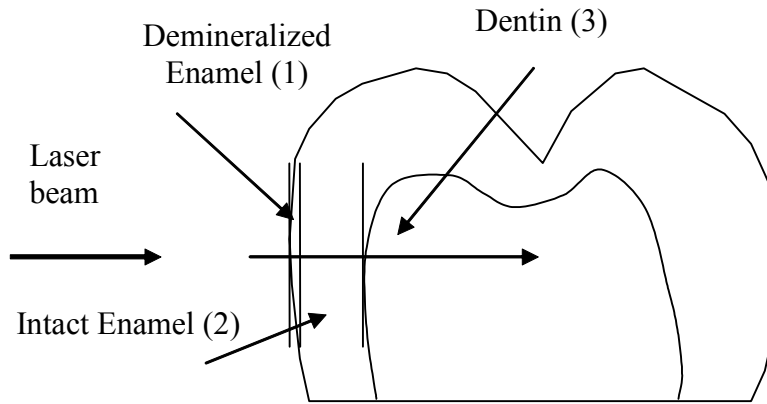


Fig. 3. Tooth structure.

The one-dimensional coherent photon-density field takes into account reduction of the incident intensity due to scattering and absorption:

$$\Psi_c = I_0 (1 - R) \exp(-\mu_t z) \quad (2)$$

where I_0 is the laser intensity, R is the reflectivity of the outermost turbid medium (enamel), and

$$\mu_t = \mu_a + \mu_s \quad (3)$$

Here, μ_t is the total attenuation coefficient of layer i , which includes the absorption coefficient, μ_a [m^{-1}], and the scattering coefficient, μ_s [m^{-1}], of the medium.

The dc form of the diffuse component for every layer can be written as:⁵

$$\frac{d^2}{dz^2} \Psi_d(z) - 3\mu_a \mu_t' \Psi_d(z) = -\frac{1}{D} G(z) \quad (4)$$

where the forcing function G is equal to:

$$G(z) = \frac{1}{2}(1-R)I_0\mu_s \frac{\mu_t + g\mu_a}{\mu_t - g\mu_s} \exp(-\mu_t z) \quad (5)$$

Boundary conditions were applied as published by the authors,^{5,14} with the continuity of heat and flux between the boundaries. Yet, it should be noted here that no distinct boundary exists between the demineralized layer and the healthy enamel. There is a gradual change in enamel conditions running from demineralized to healthy enamel, so the adopted layered structure of enamel should be considered as an approximation only.

The optical absorption coefficient was defined as:

$$D = \frac{1}{3\mu_t'} \quad (6)$$

where the reduced attenuation coefficient is:

$$\mu_t' = \mu_a + (1-g)\mu_s \quad (6)$$

For tissues, the reduced attenuation coefficient is much smaller than the total attenuation coefficient, Eq. (3), due to a high value of the mean cosine of the scattering angle g , which is close to unity for highly scattering turbid media.¹⁵

The total diffuse photon density field, Eq. (1), is a source of the much more slowly propagating thermal-wave field given by:

$$\frac{d^2}{dz^2} T_i(z; \omega) - \sigma_i^2 T_i(z; \omega) = -\eta_{NR} \frac{\mu_{a_i}}{\kappa_i} \Psi_{t_i}(z; \omega) \quad (7)$$

where

$$\sigma_i = \sqrt{\frac{i\omega}{\alpha_i}} \quad (8)$$

is the thermal-wave number, [m^{-1}], which depends on the modulation frequency and thermal diffusivity α , [m^2s^{-1}], of the i -th layer. During theoretical modeling three-layer structure was adopted as depicted in Fig. 4. At the air-solid interface, $z = 0$, third kind boundary conditions were adopted, whereas, continuity of thermal-wave field and flux between the boundaries were assumed at all remaining interfaces, resulting in the thermal-wave field distribution as a function of depth and modulation frequency.

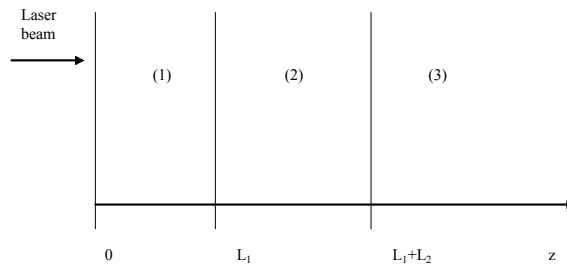


Fig. 4. Three-layer scheme.

The resulting theoretical PTR signal is a function of the effective mean infrared absorption coefficient of the medium μ_{IR} and the thermal-wave field obtained as a solution of Eq. (8). The three-layered approach gives:

$$V_{PTR} = c\mu_{IR} \left[\int_0^{L_1} T_1(z; \omega) \exp(-\mu_{IR}z) dz + \int_{L_1}^{L_1+L_2} T_2(z; \omega) \exp(-\mu_{IR}z) dz + \int_{L_1+L_2}^{\infty} T_3(z; \omega) \exp(-\mu_{IR}z) dz \right] \quad (9)$$

The instrumental constant c was normalized out by dividing experimental and theoretical curves by the first point of the intact enamel frequency scans.

4. RESULTS AND DISCUSSION

The experimental results for the PTR frequency scans before and after 2 and 4 days of tooth demineralization are shown in Fig. 5. The artificial demineralization solution applied in the experiments simulates the natural demineralization process, which is very slow. However, even after 2 days of treatment, the PTR signal shows clear change, indicating high sensitivity of the method to incipient demineralization. After 4 days of demineralization, the sample was sectioned and underwent Transversal Micro-Radiography (TMR) measurements, which showed that the thickness of the demineralized layer was equal to 48.2 μm . This tiny layer could not be detected visually or with X-ray examination. This makes the PTR method a very promising tool for the detection of incipient changes in the enamel.

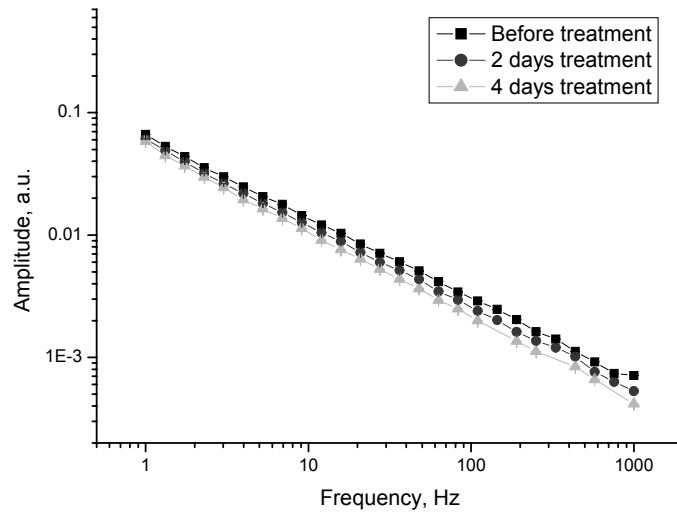
At high frequencies, the optical energy deposition within one period decreases, so the resulting thermal energy content and flux emitted from the sample decreases proportionally. This leads to lower amplitude values and very low signal-to-noise ratio, especially for the phase, which undergoes relatively small changes compared to amplitude (note the linear scale in Fig. 5b as opposed to logarithmic scale in Fig. 5a) and is more sensitive to the changes in sample properties. This phenomenon is clearly indicated in Fig. 5 showing large error bars of the phase curves at high frequencies. Therefore, only low- and middle-frequency ranges were used in the theoretical fittings. The thermal and optical parameters of intact enamel and dentin used as initial values for the fittings are summarized in Table 1.

First, the analysis of the impact of the dentin layer on the theoretical description of the process was investigated. To this end, the experimental curves for the intact tooth sample were fitted using Eq. (9) with $L_1 = 0$, $L_2 = \text{finite}$ (fitted number), $L_3 = \infty$, i.e. the enamel layer has finite thickness and dentin properties are taken into account. Then, the theoretical signal was calculated with the obtained properties and infinite enamel thickness $L_2 = \infty$, so the dentin properties become negligible in this case.

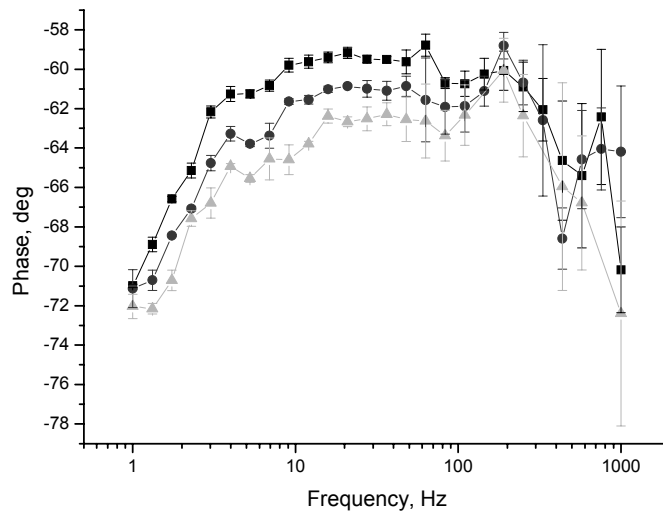
The results of the comparison of the calculations are presented in Fig. 6. There is significant difference between the curves, especially in the low frequency region of the phase curve, where the thermal diffusion depth λ is large. Here, the thermal-wave field propagates more deeply into the sample. Consequently, the first approach, which takes into account the dentin layer, can describe the experimental data better, especially for the sensitive phase curve. Therefore, it becomes necessary to include the dentin layer in computational fits, although it makes the calculations slightly more complicated.

Table 1. The initial parameters of intact enamel and dentin used in the fits.¹⁶⁻¹⁸

	Optical absorption coefficient μ_a, m^{-1}	Optical scattering coefficient μ_s, m^{-1}	Thermal diffusivity $\alpha, \text{m}^2/\text{s}$	Thermal conductivity $\kappa, \text{W/mK}$
Enamel	<100	6000±1800	$(4.2 - 4.69) \cdot 10^{-7}$	0.913-0.926
Dentin	300-400	28000±8400	$(1.87 - 2.6) \cdot 10^{-7}$	0.577-0.623

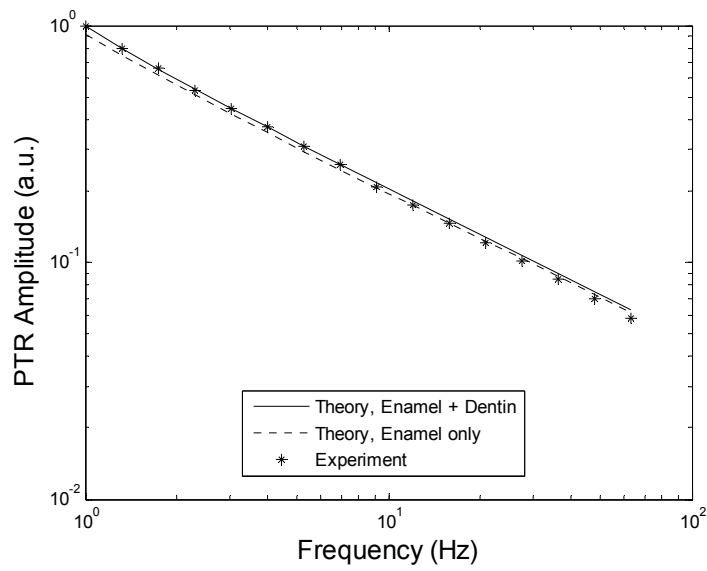


(a)

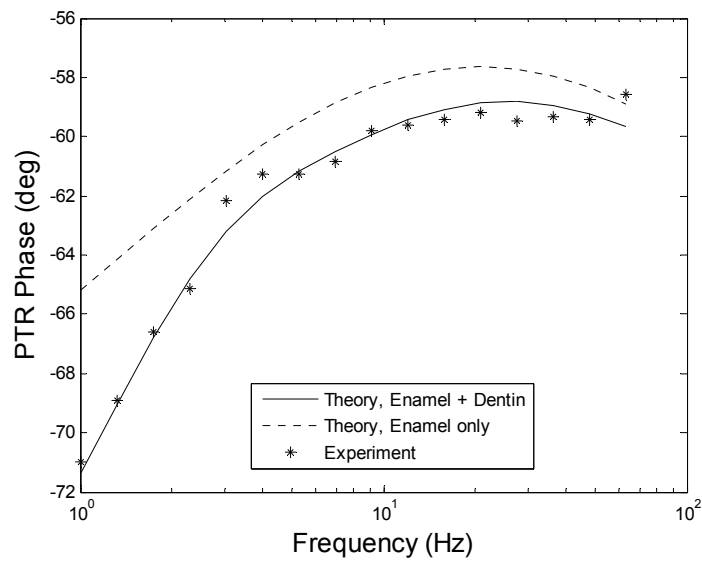


(b)

Fig. 5. PTR frequency scans, (a) amplitude and (b) phase, before treatment and after 2 and 4 days of treatment.



(a)

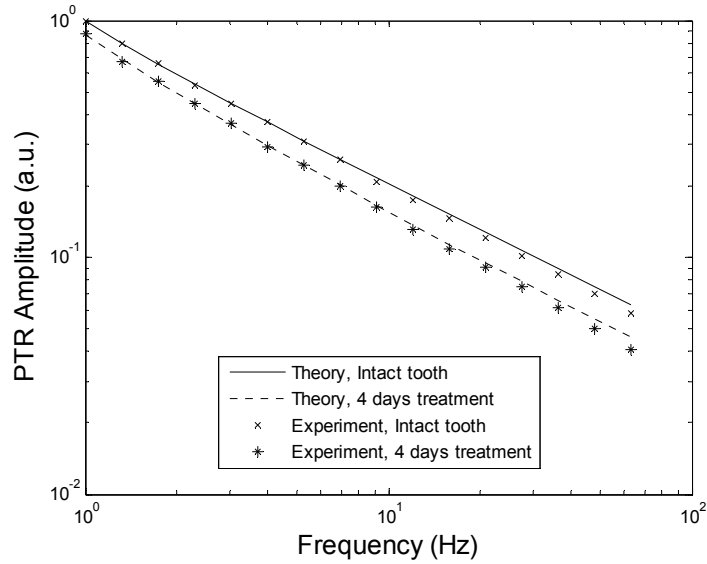


(b)

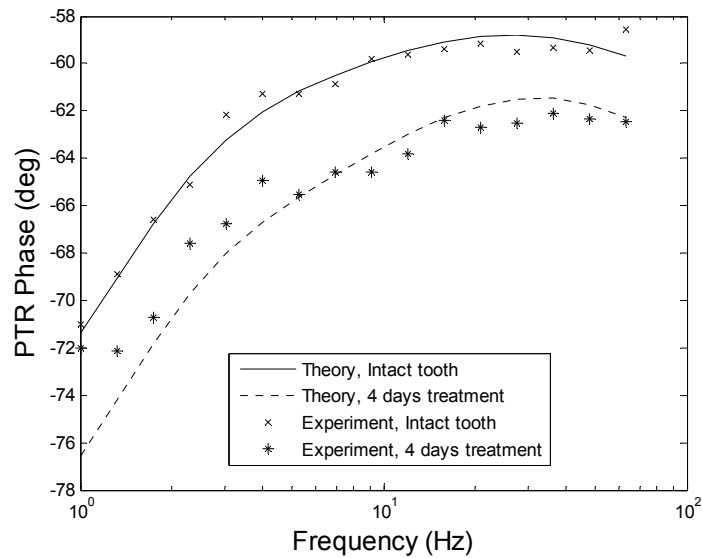
Fig. 6. Amplitude (a) and phase (b) of experimental and fitted curves for the intact tooth signal. Fitted parameters of enamel: $\mu_a = 100 \text{ m}^{-1}$, $\mu_s = 4000 \text{ m}^{-1}$, $\alpha = 4.2 \times 10^{-7} \text{ m}^2/\text{s}$, $\kappa = 0.92 \text{ W/mK}$. Fitted parameters of dentin: $\mu_a = 300 \text{ m}^{-1}$, $\mu_s = 36000 \text{ m}^{-1}$, $\alpha = 1.87 \times 10^{-7} \text{ m}^2/\text{s}$, $\kappa = 0.6 \text{ W/mK}$. Demineralized enamel thickness $L_1 = 0 \text{ }\mu\text{m}$, fitted intact enamel thickness $L_2 = 648.44 \text{ }\mu\text{m}$ (according to SEM image, the thickness in the measured region varies between about 600 to 700 μm). Fitted mean infrared absorption coefficient $\mu_{IR} = 101554 \text{ m}^{-1}$.

The frequency scans of the tooth sample treated for 4 days were fitted (Fig. 7) using the three-layer theoretical model Eq. (9) and the fitted optical and thermal parameters of intact enamel and dentin. The thickness of the demineralized enamel in the fits is equal to $L_1 = 48.2 \text{ }\mu\text{m}$, according to the TMR measurements. The parameters of the demineralized layer

obtained as a result of the fits show decrease in the optical absorption coefficient after demineralization. This can be caused by increasing porosity, which decreases the number of absorbing particles in the layer. The same reason can lead to the decrease in the thermal parameters of the demineralized layer. Although the resulting infrared absorption coefficient didn't change, this is probably due to the fact that the mean infrared absorption in the entire sample would tend to mask the ultrathin layer contributions to its overall value. The investigation of these phenomena and the accuracy of the fitting procedure is the subject of future work.



(a)



(b)

Fig. 7. Amplitude (a) and phase (b) of experimental and fitted curves for tooth demineralized for 4 days. Fitted parameters of demineralized enamel: $\mu_a = 2.3 \text{ m}^{-1}$, $\mu_s = 4000 \text{ m}^{-1}$, $\alpha = 1.4 \times 10^{-7} \text{ m}^2/\text{s}$, $\kappa = 0.56 \text{ W/mK}$. Parameters of intact enamel and dentin are the same as in Fig.6. Demineralized enamel thickness $L_1 = 48.2 \text{ }\mu\text{m}$, intact enamel thickness $L_2 = 648.44 \text{ }\mu\text{m}$. Fitted mean infrared absorption coefficient $\mu_{IR} = 101554 \text{ m}^{-1}$.

5. CONCLUSIONS

The results of the study demonstrated the potential of the photothermal radiometry to detect incipient changes in hard biological tissues such as human dental enamel. The experiments showed very high sensitivity of the measured signal to the changes in the enamel structure and properties, emphasizing the clinical capabilities of the method. The developed theoretical model, featuring coupled diffuse-photon-density-wave and thermal-wave fields, allowed fitting thermal and optical properties of tooth sample layers. The theoretical analysis showed that dentin properties should be taken into account in the fits.

ACKNOWLEDGEMENTS

The support of the Ontario Centres of Excellence (OCE) and the Center for Materials and Manufacturing (CMM) is gratefully acknowledged. We are thankful to G. Arvizu and A. Esteban Gomez for their help during the experiments.

REFERENCES

- ¹ D. Fried, W. Seka, R.E. Glens, J.D.B. Featherstone, *Opt. Eng.* **35**, 1976-1984 (1996).
- ² M.J. Zuerlin, D. Fried, J.D.B. Featherstone, W. Seka, *IEEE J. Quantum Electron.* **5**, 1083-1089 (1999).
- ³ S.A. Prahl, I.A. Vitkin, U. Bruggemann, B.C. Wilson, R.R. Anderson, *Phys. Med. Biol.* **37**, 1203-1217 (1992).
- ⁴ A. Mandelis, C. Feng, *Phys. Rev. E* **65**, 021909 (2002).
- ⁵ L. Nocolaides, Y. Chan, A. Mandelis, I.A. Vitkin, *J. Opt. Soc. Am. A* **18**, 2548-2556 (2001).
- ⁶ L. Nocolaides, C. Feng, A. Mandelis, S.H. Abrams, *Appl. Opt.* **41**, 768-777 (2002).
- ⁷ J.M. Schmitt, G.X. Zhou, E.C. Walker, R.T. Wall, *J. Opt. Soc. Am. A* **7**, 2141-2153 (1990).
- ⁸ L.O. Svaasand, T. Spott, J.B. Fishkin, T. Pham, B.J. Tromberg, M.W. Berns, *Phys. Med. Biol.* **44**, 801-813 (1999).
- ⁹ A. Kienle, M.S. Patterson, N. Dognitz, R. Bays, G. Wagnieres, H. van den Bergh, *Appl. Opt.* **37**, 779-791 (1998).
- ¹⁰ A.D. Kim, M. Moscoso, *J. Bio. Opt.* **10**, 034015 (2005).
- ¹¹ T.J. Farrell, M.S. Patterson, M. Essenpreis, *Appl. Opt.* **37**, 1958-1972 (1998).
- ¹² G. Alexandrakis, T.J. Farrell, M.S. Patterson, *Appl. Opt.* **37**, 7401-7409 (1998).
- ¹³ A. Kienle, T. Glanzmann, G. Wagnieres, H. van den Bergh, *Appl. Opt.* **37**, 6852-6862 (1998).
- ¹⁴ Z. A. J. Groenhuis, H. A. Ferwerda, and J. J. Ten Bosch, *Appl. Opt.* **22**, 2456-2462 (1983).
- ¹⁵ A. Ishimaru, *Appl. Opt.* **28**, 2210-2215 (1989).
- ¹⁶ D.Fried, R.E. Glens, J.D.B. Featherstone, W. Seka, *Appl. Opt.* **34**, 1278-1285 (1995).
- ¹⁷ W.S. Brown, W.A. Dewey, H.R. Jacobs, *J. Dent. Res.* **49**, 752 (1970).
- ¹⁸ M. Braden, *Arch. Oral Biol.* **9**, 479-486 (1964).